

Influence of surface contamination on electric field distribution of insulators

Xingcai Li(李兴财), Yingge Liu(刘滢格), and Juan Wang(王娟)

Citation: Chin. Phys. B, 2025, 34 (**3**): 034101. DOI: 10.1088/1674-1056/ada54d
Journal homepage: http://cpb.iphy.ac.cn; http://iopscience.iop.org/cpb

What follows is a list of articles you may be interested in

Effect of boundary slip on electroosmotic flow in a curved rectangular microchannel

Yong-Bo Liu(刘勇波)1,2
Chin. Phys. B, 2024, 33 (**7**): 074101. DOI: 10.1088/1674-1056/ad3340

Ultra-wideband surface plasmonic bandpass filter with extremely wide upper-band rejection

Xue-Wei Zhang(张雪伟), Shao-Bin Liu(刘少斌), Qi-Ming Yu(余奇明), Ling-Ling Wang(王玲玲), Kun Liao(廖昆), and Jian Lou(娄健)
Chin. Phys. B, 2022, 31 (**11**): 114101. DOI: 10.1088/1674-1056/ac6015

Electron beam modeling and analyses of the electric field distribution and space charge effect

Yueling Jiang(蒋越凌) and Quanlin Dong(董全林)
Chin. Phys. B, 2022, 31 (**5**): 054103. DOI: 10.1088/1674-1056/ac3d84

High-confinement ultra-wideband bandpass filter using compact folded slotline spoof surface plasmon polaritons

Xue-Wei Zhang(张雪伟), Shao-Bin Liu(刘少斌), Ling-Ling Wang(王玲玲), Qi-Ming Yu (余奇明), Jian-Lou(娄健), and Shi-Ning Sun(孙世宁)
Chin. Phys. B, 2022, 31 (**1**): 014102. DOI: 10.1088/1674-1056/ac22a2

Reciprocity principle-based model for shielding effectiveness prediction of a rectangular cavity with a covered aperture

Jiao Chong-Qing (焦重庆), Li Yue-Yue (李月月)
Chin. Phys. B, 2015, 24 (**10**): 104101. DOI: 10.1088/1674-1056/24/10/104101

Influence of surface contamination on electric field distribution of insulators

Xingcai Li(李兴财)[1,†], Yingge Liu(刘滢格)[1], and Juan Wang(王娟)[1,2]

[1] *School of Physics, Ningxia University, Yinchuan* 750021, *China*
[2] *Xinhua College, Ningxia University, Yinchuan* 750021, *China*

(Received 26 October 2024; revised manuscript received 11 December 2024; accepted manuscript online 3 January 2025)

Atmospheric particle adsorption on insulator surfaces, coupled with humid environments, significantly affects contamination flashover, necessitating a clear understanding of the electric field distribution on insulator surfaces with adsorbed particles. This is crucial for accurately assessing insulator safety and informing critical decision-making. Although previous research has demonstrated that particle arrangement significantly influences the electric field distribution around transmission lines, an in-depth analysis of its effects on insulator surfaces remains lacking. To address this gap, this study establishes a composite insulator model to examine how three types of spherical contamination layers affect the electric field distribution on insulator surfaces under varying environmental conditions. The results reveal that in dry environments, the electric field strength at the apex of single-particle contamination layers increases with the particle size and relative permittivity. For the double-particle contamination layers, the electric field intensity on the insulator surface decreases as the particle spacing increases, and larger particles are more likely to attract smaller charged particles. For triple-particle contamination layers arranged in a triangular pattern, the maximum surface field strength is nearly double that of the chain-arranged particles. Furthermore, within the chain-arranged triple-particle contamination layers, a large–small–large size arrangement has a more pronounced impact on the surface electric field than a small–large–small size arrangement. In humid environments, the surface electric field strength of insulators decreases with increasing contamination levels. These findings are of significant theoretical and practical importance for ensuring the safe operation of power systems.

Keywords: composite insulator, electric field distribution, contamination, humid environment, arrangement pattern

PACS: 41.20.Cv, 92.60.Mt, 52.80.Mg, 84.70.+p

DOI: 10.1088/1674-1056/ada54d **CSTR:** 32038.14.CPB.ada54d

1. Introduction

As critical insulating components for open-air substations and overhead high-voltage transmission lines, insulators must endure various mechanical stresses while providing electrical insulation.[1] The surfaces of outdoor insulators are subject to contamination by natural salts, industrial pollutants, and dust.[2,3] During normal operation, the high field strength around insulators leads to the significant adsorption of particulate matter, severely affecting the surface morphology and increasing the likelihood of contamination flashover. This can result in pollution flashover incidents, compromising the reliability and safe operation of power systems.[4] Furthermore, humid environments can alter the electromagnetic environment around insulating equipment.[3,5] The adsorption of atmospheric particles can exacerbate humid contamination flashover phenomena, thereby increasing maintenance costs.[6,7] Statistical reports on insulator pollution flashover incidents[8,9] indicate that surface contamination is the primary cause of insulator flashover accidents. Therefore, by examining the components of contamination and their arrangement patterns, we can study the electric field distribution patterns caused by surface contamination on insulators to understand the mechanisms of insulator flashover.[9] This study provides a crucial theoretical foundation for addressing pollution flashover issues and ensuring the normal operation of transmission systems under various environmental conditions.

To investigate the mechanism of flashover due to contamination on insulators, researchers both domestically and internationally have conducted extensive studies on various aspects. These include the potential and electric field distribution on contaminated insulator surfaces,[10,11] dynamic contamination process,[12–14] electric field distribution under different environmental conditions,[15,16] electric field analysis of composite insulators,[12,14,17] and characteristics of the electromagnetic environment around insulators under clean conditions.[18,19] Numerical simulation methods are predominantly used in electric field studies. Compared to experimental measurement methods, numerical simulations not only shorten the testing cycle and reduce costs but also ensure the reproducibility of results, making them widely applicable in engineering design. Some researchers have analyzed the impact of different contaminants on the electric field distribution on insulator surfaces. Peng *et al.*[20] focused on rooftop insula-

[†]Corresponding author. E-mail: nxulixc2011@126.com

© 2025 Chinese Physical Society and IOP Publishing Ltd. All rights, including for text and data mining, AI training, and similar technologies, are reserved.

tors, and analyzed the impact of parameters such as the water droplet radius, number, and position on the surface electric field of insulators. Gao *et al.*[21] investigated the distortion patterns of the electric field on insulators influenced by the distribution of algae and external weather conditions. Their findings revealed that electric field distortion was most severe when algae were distributed at the high-voltage end, whereas there is negligible change in the electric field distribution when algae were located on the skirts at the low-voltage end. Ma *et al.*[15] used multiphysics simulation software to establish an FOBG-25 contact network insulator model and investigated the surface and spatial potential and electric field distribution of contaminated insulators under high conductivity salt–alkali fog conditions. Hu *et al.*[22] studied the electric field distribution of composite insulators coated with electrically heated paint exhibiting a breaking effect. The results showed that the more interspersed the dry zones and paint distribution, the less pronounced the electric field distribution. Xiang *et al.* conducted an analysis and calculation of the electric field on insulator surfaces covered with non-uniform contamination layers. They discovered that the axial non-uniformity of contamination distribution on the insulator surface affects the surface electric field intensity.[23] Yu *et al.* used finite element analysis to study the effects of factors such as the position, width, and number of dry bands on the electric field of insulators. They determined the electric field intensity on insulator surfaces under various conditions.[24] These findings provide a theoretical basis for reducing the occurrence of pollution flashover in insulators. Lü *et al.* investigated the effects of water droplet radius, spacing, and dielectric constant on the electric field distortion of clean insulators.[25] Gao *et al.*[26] used finite element numerical simulation to calculate the electric field distribution of a single porcelain insulator under non-uniform contamination. Lü's team[27] discussed the factors influencing the analysis of porcelain insulator electric field distribution using the finite element method and identified the applicable scenarios for the electro-quasi-static field. Liu *et al.*[28] analyzed the adhesion characteristics of smog particles, leakage current, and flashover voltage under different smog parameters. Qiao *et al.*[29] conducted simulation experiments to determine the AC breakdown voltage of composite insulators under five natural conditions: dry, frost, cold fog contamination, glazed ice without icicles, and glazed ice with icicles. Liu *et al.*[17] established a natural contamination accumulation system and analyzed the microstructural characteristics of surface insulators under different conditions. They proposed an electric dipole model of aerosol clusters to explain the contamination distribution characteristics on the surfaces of DC-charged insulators. Frizzo *et al.*[30] considered the effects of contamination, cracks, and bird nests on the electric field distribution on insulator surfaces. Using software simulations, they obtained the surface field intensity of insulators under these various conditions and evaluated the state of insulators in different scenarios. Abd Rahman *et al.*[31] investigated the operating environment of insulators, focusing on the impact of relative humidity on the surface electric field intensity of insulators. They established a correlation between these factors and confirmed that sharp edges and material thickness are among the factors that influence the electric field intensity of insulators. Ndoumbe *et al.*[32] conducted simulation of the surface electric field on dry and damp porcelain and composite insulators under three different high-voltage conditions. They also analyzed the impact of corona rings on the electric field distribution on insulator surfaces under the same conditions. Krzma *et al.*[33] conducted a two-dimensional (2D) simulation study on the electric field distribution of uniformly contaminated composite insulators. Aouabed *et al.*[34] used finite element simulation software to model the impact of water droplets of different shapes on the electric field distribution of insulators. Salem *et al.*[35] presented a dynamic model that simulated and tested the flashover of polluted insulators using HV voltage. The results showed that the effect of the pollution layer conductivity on the electric field was significant. Ahmadi-veshki *et al.*[36] conducted extensive FOV tests on aged SiR insulators under varying humidity and contamination conditions and proposed a new mathematical model for insulator reliability at different humidity levels. Kim *et al.*[37] analyzed the deterioration of high-voltage insulators in service areas due to contamination factors. Fadaeeasrami *et al.*[38] performed finite element simulations on elliptical ring-contaminated 230-kV insulator strings, demonstrating that variations in the diameter, thickness, and conductivity of the elliptical contamination layer are crucial to the insulation performance of high-voltage insulators.

From the above discussion, it is evident that most studies have focused on numerical simulations and the experimental validation of single-layer uniform contamination particles. There is a scarcity of literature on the electric field distribution of high-voltage transmission lines and composite insulators under different contamination configurations, as well as on the impact of droplets with varying contamination levels in humid environments. In reality, the contamination of transmission equipment has varying degrees of non-uniformity. Simplified models of different contamination configurations include particles of different sizes arranged in various patterns. Liu *et al.*'s research indicated that the arrangement and distribution of adsorbed particles on transmission conductors can significantly enhance the surrounding electric field and alter its distribution.[39] However, there is still a lack of research on the impact of the particle arrangement on the electric field of insulator surfaces. Given the relatively small distance between the skirts of insulators, changes in the electric field in-

tensity and distribution around each skirt can severely impact the pollution flashover of the insulators. Therefore, analyzing the characteristics of the electric field distribution under different contamination configurations on insulator surfaces in various environments is of significant practical importance.

2. Model construction

2.1. Basic principle

The calculation of the electric field distribution in this study is based on the Poisson equation. Expressed in the form of a differential equation, it provides the relationship between the potential φ and charge density ρ, as shown in Eq. (1). COMSOL finite element simulation software is utilized to solve for the electric field intensity on the surface of the composite insulators under contamination conditions, ensuring that the computational domain satisfied charge conservation

$$\nabla^2\varphi = \frac{\partial^2\varphi}{\partial x^2} + \frac{\partial^2\varphi}{\partial y^2} + \frac{\partial^2\varphi}{\partial z^2} = -\frac{\rho}{\varepsilon_0}. \tag{1}$$

The electric field of the composite insulators satisfies the following Eqs. (2) and (3). The constitutive relation of the electric field uses the relative permittivity and satisfies Eq. (4).

$$\boldsymbol{\nabla}\cdot\boldsymbol{D} = \rho_v, \tag{2}$$

$$\boldsymbol{E} = -\boldsymbol{\nabla}V, \tag{3}$$

$$\boldsymbol{D} = \varepsilon_0\varepsilon_{\mathrm{r}}\boldsymbol{E}. \tag{4}$$

2.2. Geometric model

This study established a model of composite insulators under pollution conditions, as illustrated in Fig. 1, by employing a 1:1 geometric modeling approach and hybrid mesh generation. The computational domain and surface of the insulator were discretized and solved using this methodology.

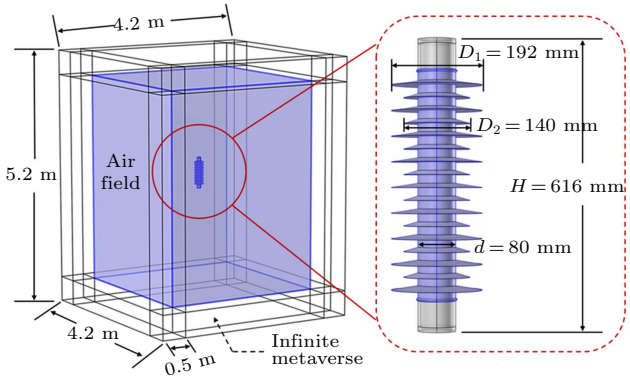


Fig. 1. Calculation domain diagram of composite insulator model under clean condition.

Solving the surface electric field of composite insulators is an open domain problem. The finite element method (FEM) was used to establish an artificial boundary at a substantial distance from the composite insulator. Considering practical conditions, the ground was assumed to be a good conductor, and the potential at the artificial ground boundary was set to zero. To ensure that the air domain boundary closely approximates infinity, a virtual domain was introduced at the artificial boundary, effectively addressing the calculation of the electric field in an infinite space.[15,25,40] Additionally, based on the spatial domain selection method proposed in existing research,[9] and considering the computational efficiency of the model, the computational domain was ultimately determined to be 4.2 m×4.2 m×5.2 m. The size of this model and the computational domain remained constant throughout the subsequent calculations.

2.3. Grid division and condition setting

In this study, a combination of structured and unstructured mesh techniques was utilized to achieve an ultra-fine mesh division of the model. The overall mesh profile of the model is shown in Fig. 2. The final model achieved an average mesh quality of 0.6683.

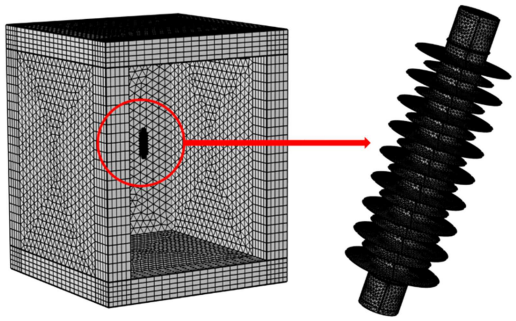


Fig. 2. Grid subdivision diagram of three-dimensional insulator model.

The composite insulator model employs finite boundaries to substitute for infinite boundaries, constrained by applying asymptotic boundary conditions. The boundary conditions for the composite insulator are given by Eq. (5), and at the continuous interface of different media, they satisfy Eq. (6).

$$\boldsymbol{n}\cdot(\boldsymbol{D}_1 - \boldsymbol{D}_2) = 0, \tag{5}$$

$$\begin{cases} \varphi|_{l_0} = U, \\ \varphi|_{l_1} = 0. \end{cases} \tag{6}$$

The electrostatic field module was used to calculate the electric field of composite insulators under clean and polluted conditions in this study. The voltage parameters were set based on the research of Wang[9] on catenary insulators. According to the requirements of the domestic railway power supply departments, the maximum voltage of the catenary transmission line must not exceed 29 kV, and the peak AC voltage is $29\times\sqrt{2}\approx 41$ kV. Therefore, the voltage at the high-voltage end of the insulator was set to 41 kV, while the low-voltage end was grounded (0 kV). The specific parameters are shown in Table 1.[41]

Table 1. Material setting parameters of each component of insulator.

Component	Material	Relative dielectric constant	Conductivity (S/m)
Air domain	air (drying)	1.006	0
Core rod	glass fiber	2.09	10^{-14}
Insulation sheath	silicone rubber	3.5	2.35×10^{-12}
Hardware	CZ42 (aluminum alloy)	1×10^{8}	6×10^{7}

3. Model analysis

Based on the above data, a simulation was performed to calculate the surface electric field of a clean insulator. The surface potential and electric field of the insulator is shown in Fig. 3. In order to verify the authenticity and accuracy of this model, this study uses image processing to compare with existing research,[9] and obtains the comparative verification results shown in Fig. 3(a). The mean square error (MSE) is 9.6329, indicating that the two models are in good agreement, but there are local errors. The average absolute error (MAE) is 1.4880, which further indicates that the error between the two models is relatively small. Through the error distribution histogram, it is not difficult to find that the error values are concentrated in a small range, and the error values of most pixels are low, which indicates that the two models have a good agreement on the whole. The long tail phenomenon, that is, the error value of a few pixels is large, may be due to the incomplete overlap of the target area boundary. The relative error indexes Relative MSE and MAE are 0.3066 and 0.2655, respectively, that is, the error accounts for a small proportion of the normalized range, which further proves that the model is in good agreement with the existing research.

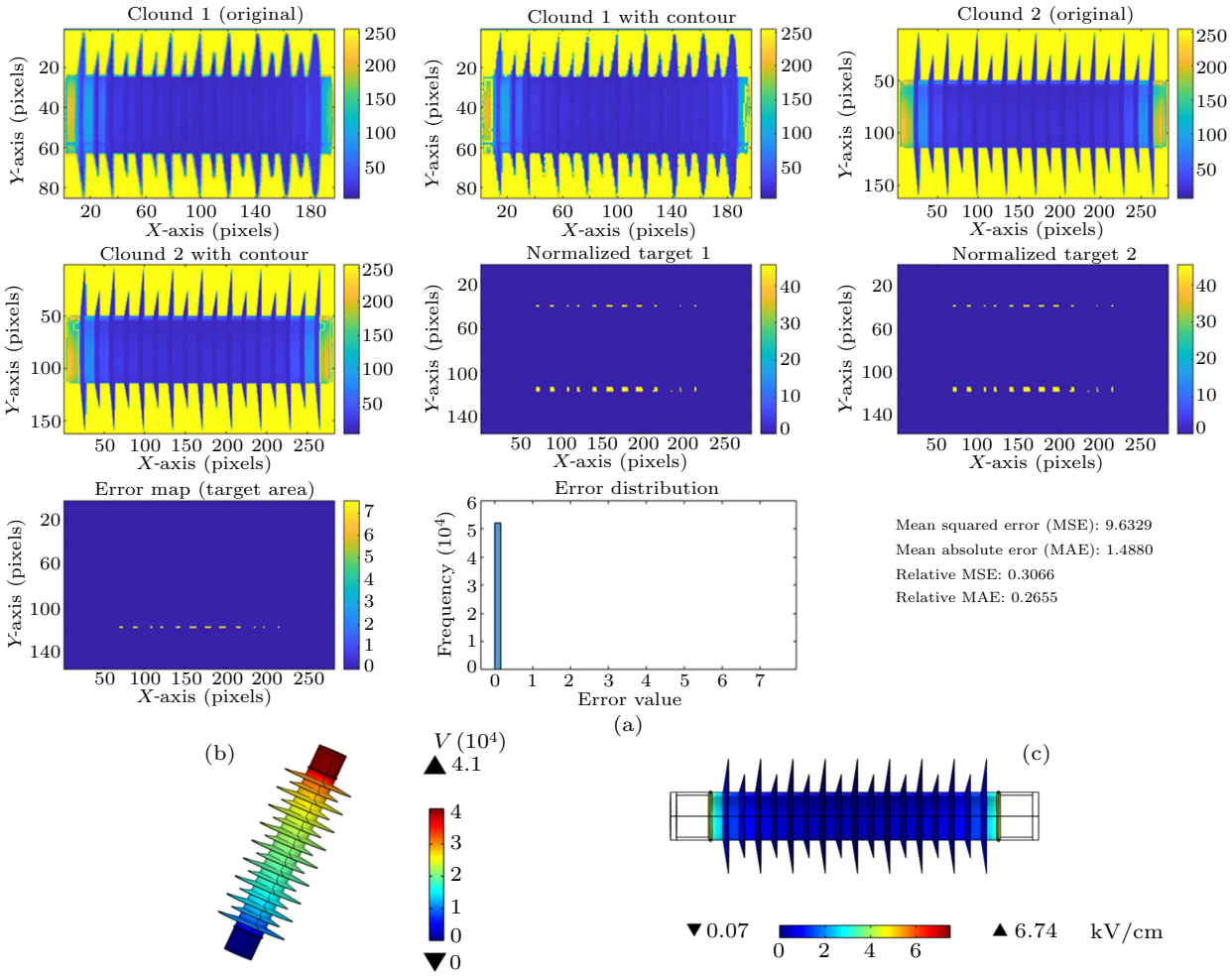


Fig. 3. Model verification and calculation results diagram: (a) model validation comparative analysis diagram, (b) electric potential distribution, and (c) electric field distribution.

In Fig. 3(b), the maximum surface potential of the insulator is 41 kV, which appears at the high-voltage side of the insulator at the metal fitting. The minimum value is 0, which occurs at the low-voltage side of the insulator at the metal fitting. The radial distribution of the surface potential is uniform, while axially it shows a decreasing trend. As depicted, the potential gradually decreases from the high-voltage side to the low-voltage side, eventually reaching zero. The potential changes dramatically at the upper metal fitting, decreases smoothly across the insulating sheath, and changes drastically again at the tail of the insulator until it reaches zero.

To more precisely illustrate the variation of the electric

field, the change in electric field strength with the creepage distance (it is the shortest path along the insulator surface between the upper and lower hardware) was calculated, resulting in the curve shown in Fig. 4. Combining Figs. 3(c) and 4, it can be seen that the electric field strength on the surface of the silicone rubber is characterized by higher values at both sides and lower values in the middle. The field strength at the high-voltage side is greater than that at the low-voltage side, with the field strength of the middle section differing by an order of magnitude from that at the sides. The field strength in the middle section of the insulator generally remains between 0.2 kV/cm and 0.5 kV/cm, with relatively small fluctuations. The field distribution diagram indicated that the electric field strength on the insulator surface is higher at the gaps between the sheds, decreased as it approached the edges of the sheds, and experiencing a sudden increase at the junction points between the sheds and the sheath. The peak values (B, D, E, G) in the corresponding variation curve represent the junction points between the sheds and the sheath, whereas the valley values (C, F) correspond to the edges of the sheds.

From Fig. 4, it is evident that the electric field underwent a sudden change along segment AB. Segment BC, which corresponds to the shed section, had a slope similar to that of segment EF, indicating significant variations in the electric field within the shed section. The field strength decreases towards the edges, reaching its minimum at point C, which is the edge of the shed. Subsequently, the electric field strength gradually increases until it reaches inflection point D where the shed meets the gap. At this inflection point, there was a sudden change in field strength. Segment DE, which represents the gap between sheds, followed the same trend as segment GH. In the gap between the sheds, the electric field strength gradually decreases, with lower values closer to the middle of the insulator. The calculated results show that the electric field strength on the surface of the composite insulator follows a "U"-shaped distribution along the creepage distance. These phenomena indicate that the electric field strength on the insulator surface is more likely to experience distortion at the gaps between the sheds, whereas abrupt changes in field strength are generally unlikely at the shed edges. Consequently, this study selected the contamination accumulation area in the gaps between the sheds.

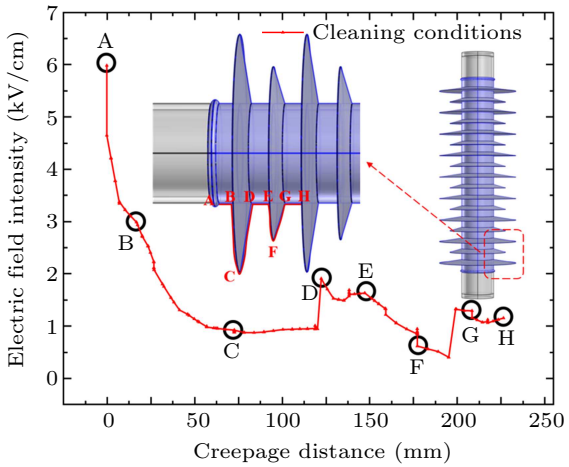


Fig. 4. The variation of electric field intensity on the surface of shed in a unit of insulator with creepage distance.

The complex aerosols in the atmosphere can easily form contamination layers of varying conditions, resulting in different degrees of change in the electrical performance of the external insulation system of the transmission lines. Therefore, this study investigates the characteristics of the electric field distribution on the insulator surface under different contamination conditions. Using spherical particles as an example, figure 5 illustrates various particle attachment scenarios: single-particle contamination with different radius and compositions, double-particle contamination with varying distances and radius, and triple-particle contamination with different arrangements and radius.

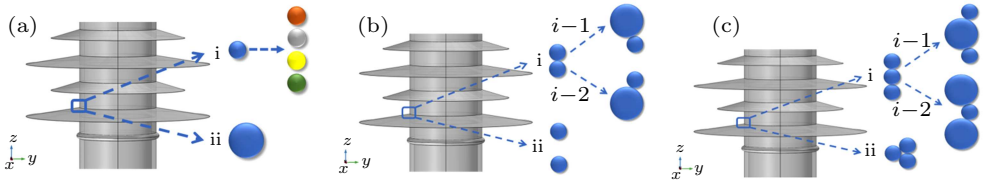


Fig. 5. Structure diagram of surface contamination on insulators: (a) single particle, (b) double particle, (c) triple particle.

4. Result and discussion

This study analyzes the electric field distribution patterns on the surface of insulators after contamination through a numerical simulation. Specifically, it examines the effects of "single particle contamination with different radius and compositions", "double particle contamination with varying distances and radius", and "triple particle contamination with different arrangements and radius". The following sections provide detailed introductions to each scenario.

4.1. The effect of single particle contamination on the electric field distribution on the insulator surface

4.1.1. The influence of the radius of filthy particles

This section investigates the effect of different particle radius on the electric field strength on the insulator surface, while keeping the relative dielectric constant of the particles

constant. Using SiO_2 aerosol particles as an example, the surface electric field strength for particles with radius ranging from 0.01 mm to 0.1 mm was calculated. The resulting surface electric field distribution cloud diagrams and maximum field strength line graphs are shown in Figs. 6 and 7, respectively.

From the electric field distribution cloud diagrams, it can be observed that the adsorption of particles at the inflection points of the sheds not only affects the maximum electric field strength on the insulator surface, but also indirectly influences the electric field strength distribution around the particles. According to the corresponding maximum field strength line graph (Fig. 7(a)), as the particle radius increased, the maximum value of the surface electric field strength also increased. However, the rate of increase gradually diminished until it stabilizes at approximately 17.03 kV/cm. From the line graph in Fig. 7(b), it can be observed that the fluctuation of the electric field intensity appears around the contaminated particles. While the electric field strength in the latter half of each shed gap is not affected by the particles, with the field values remaining almost consistent. The inset indicates that, for a fixed particle radius, the electric field strength in the front part of the insulator shed gap decreases slowly with increasing creepage distance. Except for the inflection points, the field strength fluctuated within ±0.1 kV/cm. Vertically, the surface electric field strength on the insulator sheath decreases with increasing particle radius, indicating that smaller particle radii have a more significant effect on the electric field strength on the insulator surface.

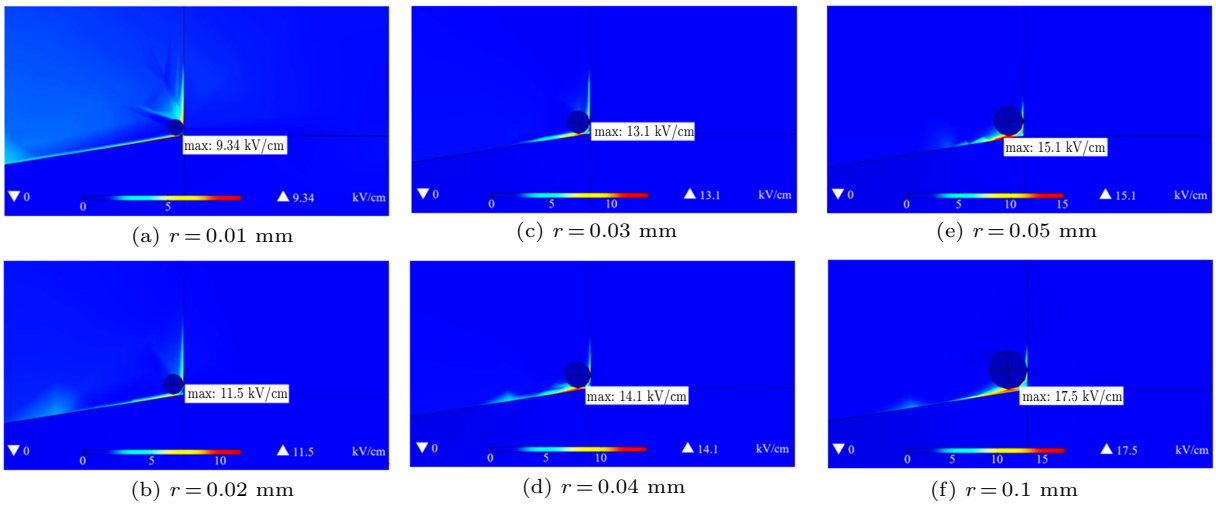


Fig. 6. The surface electric field distribution cloud diagram of single particle pollution layer with different radii.

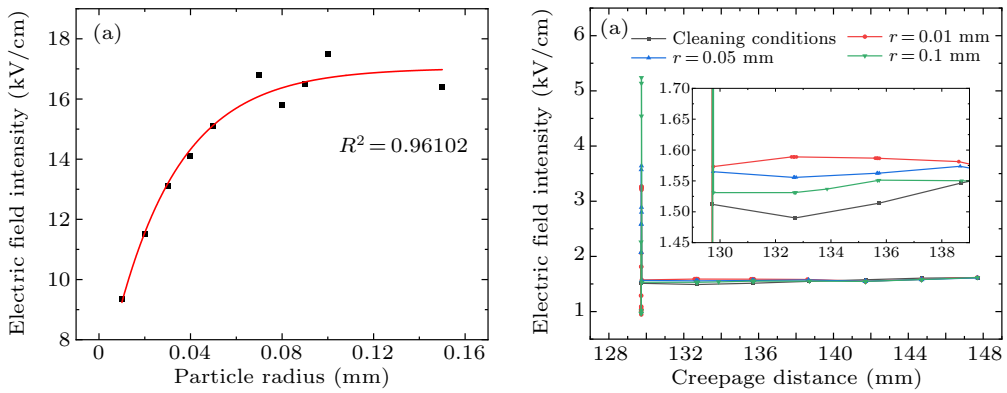


Fig. 7. Change curve of insulator surface field strength, r is the particle radius: (a) fitting curve of the maximum field strength of insulator surface with the change of particle radius, (b) curve of electric field intensity on insulator surface changing with creepage distance.

4.1.2. The influence of filthy particle composition

Extreme weather events such as sandstorms, snowstorms, and hailstorms frequently occur, causing numerous negative impacts on people's lives. These types of extreme weather can cause discharge on the surface of transmission line insulators owing to the adhesion and accumulation of contaminants, thereby affecting the safety and stability of power systems. Currently, research has been conducted to determine the content and radius distribution of contaminants in a specific region of the northwest through component detection and analysis.[9] Therefore, this section selects four major components identified in the study and includes anthracite coal contaminants from mining areas, addressing the particle pollution issues resulting from the significant increase in coal-based energy con-

sumption and the rapid increase in motor vehicle ownership in recent years.[42] The particle radius is set to 0.03 mm, and the electric field strength on the surface of the composite insulator was simulated for different particle compositions. The specific parameters of these components are listed in Table 2.[41]

It is assumed that the relative humidity of the surrounding air is small, and the filthy particles do not absorb moisture growth, therefore, the dry state will remain unchanged, and the conductivity is set to 0. In this section, the electric field on the surface of five different pollutants covered at the inflection point of the composite insulator is simulated and calculated, the field intensity distribution cloud diagram is shown in Fig. 8 and the scatter diagram of Fig. 9 are obtained.

Table 2. Material parameters of different contamination components.

Contamination components	SiO_2	$CaSO_4$	NaCl	$MgSO_4$	Anthracite
Relative dielectric constant	4.2	5.6	6.1	8.2	12.2
Density ρ (g·cm^{-3})	2.2	2.61	2.165	2.68	1.60

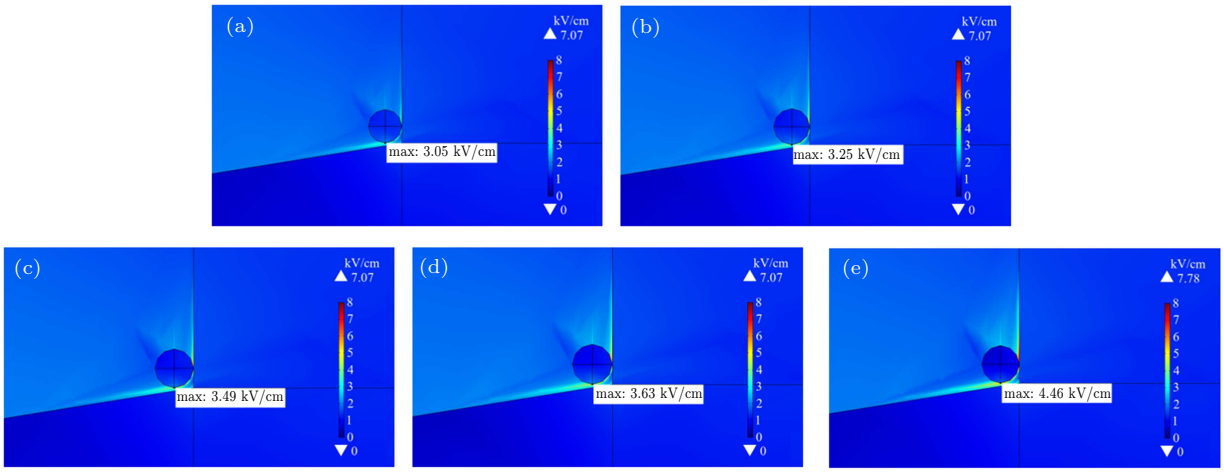


Fig. 8. Field intensity distribution in the presence of single particles with different compositions on the insulator surface: (a) SiO_2 pollution particle, (b) $CaSO_4$ pollution particle, (c) NaCl pollution particle, (d) $MgSO_4$ pollution particle, (e) anthracite pollution particle.

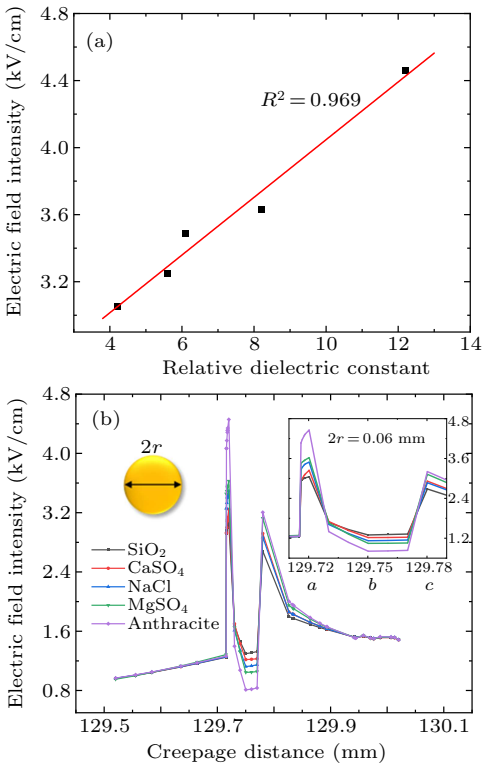


Fig. 9. The change of the maximum surface electric field on the insulator with dielectric constant and creepage distance: (a) maximum field strength with the change of relative dielectric constant, (b) surface electric field for various adhesive particles.

From the electric field distribution cloud diagrams, it is also evident that the particles significantly impact the electric field strength within small regions, particularly at the insulator gaps. Therefore, this section calculates the variation curves of the electric field strength around particles with different compositions along the creepage distance of the insulator, as shown in Fig. 9. According to the fitted data in Fig. 9(a) with $R^2 = 0.969$, the simulation results exhibit a high degree of correlation with the linear relationship, indicating a good fit. Thus, it can be concluded that they generally follow a positive correlation. Combined with the electric field distribution cloud diagrams in Fig. 8, it can be inferred that particle adsorption at the insulator-shed inflection points affects the electric field within the surrounding small regions. As the relative dielectric constant of particles with different compositions increased, the maximum electric field strength also increased.

According to Fig. 9(b), it is evident that the greater the relative dielectric constant of the contamination particles, the more pronounced the changes in the electric field strength on the insulator surface. The inset reveals that at the particle adsorption location (segment ac), the electric field strength on the insulator surface decreased as the relative dielectric constant of the particles increased. Outside the ac segment, the electric field strength on the composite insulator surface increases with the relative dielectric constant of the particles, which aligns with the fitted curve in Fig. 9(a). This phenomenon indicates

that the adsorption of single contamination particles on the insulator surface likely influences the electric field strength in different ways due to particle shape. Therefore, the impact of particle adsorption on the electric field strength of the insulator surface is not entirely negative.

4.2. The influence of double particle contamination layer on electric field distribution of insulator surface

4.2.1. The influence of different spacing of equal-sized pollution particles

This section discusses the effect of equal-sized double particles on the electric field strength of the insulator surface at different spacings. According to the single-particle model, this section will take the SiO_2 aerosol particles with a radius of $r = 0.03$ mm as an example and calculate the electric field strength of the six different spacing double particles with the spacing d of 0, 1 times the particle radius to 5 times the particle radius. A cloud map of the surface field strength distribution is shown in Fig. 10.

It can be seen from the field intensity distribution cloud diagram when two equal-sized particles are in contact with each other, the electric field intensity near the particle contact point changes abruptly, but it has little effect on the electric field intensity on the insulator surface. With an increase in particle spacing, the field strength of the insulator surface in the middle area of the two particles gradually increased. When the spacing was greater than 5 times the particle radius, the two particles had little effect on the surrounding electric field, and the field strength could be restored to the original electric field.

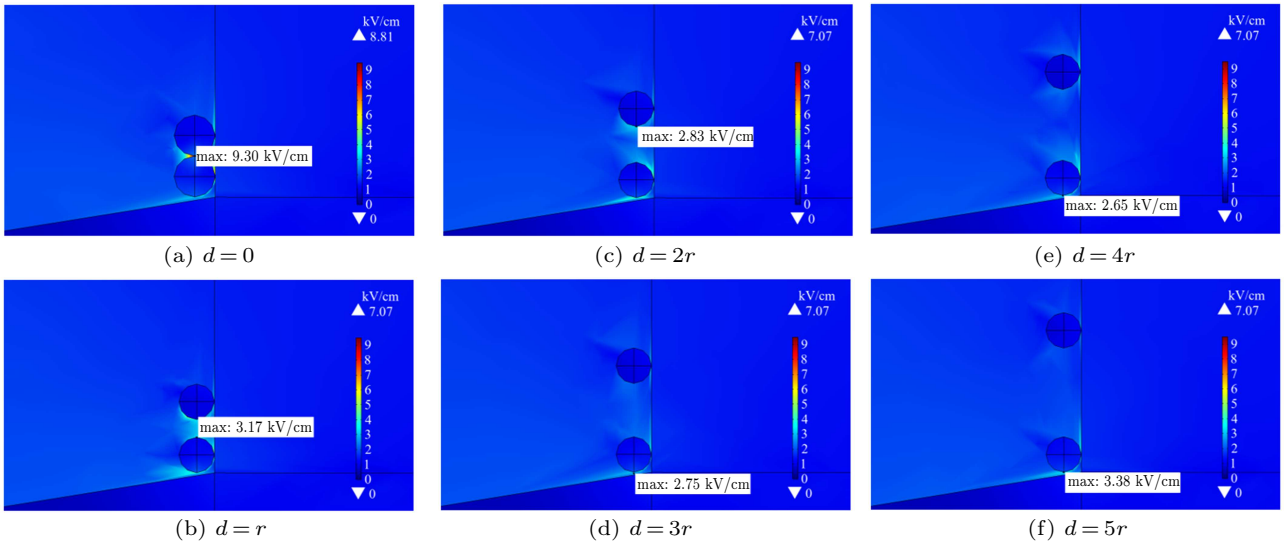


Fig. 10. The electric field distribution of insulator under different particle spacings.

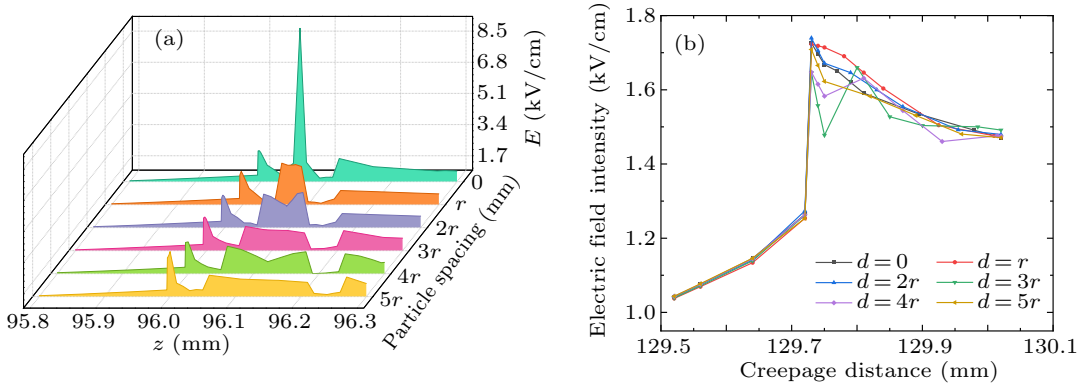


Fig. 11. The change of electric field intensity on insulator surface under different particle spacings: (a) waterfall plot of electric field intensity around particles, (b) line chart of electric field intensity change on insulator surface.

To analyze the influence of the distance between the two particles on the electric field strength of the insulator surface in more detail, this section presents the change waterfall diagram shown in Fig. 11(a), in which the two "U"-type valley areas are the positions of two equal-sized particles. From the diagram, it can be seen that the electric field distribution between particles reaches the maximum when they are in contact with each other, which is approximately 3 times the maximum field strength of the original single particle, and the electric field intensity gradually decreases with the increase in particle spacing. This indicates that with the increase of particle spacing, the mutual influence between the two particles is gradually re-

duced, and the influence of the interaction on the electric field of the insulator surface is also gradually reduced. When the spacing is greater than 3 times the radius of the particles, the effect of single particles on the electric field is greater than the interaction effect of double particles. Similarly, it can be seen that the electric field intensity decreases with the increase of the spacing between the two particles in the rear section of the upper particles, which also shows that the interaction of particles is gradually decreasing. In contrast, at the first peak, the surface electric field intensity of the insulator increases with the increase of the particle spacing, indicating that the surface electric field of the front section of the particles is weakened when the particles are in contact or close to each other, but it will protect them from corona discharge and other phenomena. Therefore, at the inflection point, the surface electric field intensity of the insulator is almost not affected by the double particles.

As mentioned above, figure 11(a) reflects the influence of different particle spacings on the surrounding electric field strength. In addition, this section also studies the change of the creepage distance of the insulator with the particle spacing, as shown in Fig. 11(b). It can be seen from the line chart that when the distance between the two particles is 0 to 2 times the radius, the electric field strength on the surface of the insulator gradually increases with the increase in the distance between the particles, and the field strength at the middle position of the two particles in the waterfall plot changes. This indicates that when the distance between the particles is less than 2 times the radius, the mutual influence and joint action of the particles have a great influence on the electric field on the surface of the insulator. When the spacing is greater than 2 times the radius, the overall electric field intensity is smaller than that when the spacing is less than 2 times the radius. Combined with the waterfall plot, it can be explained that the combined action intensity is weakened at this time, and the electric field of the insulator is affected more by the action of single particles.

4.2.2. The influence of different spacings of unequal-sized pollution particles

According to the single particle insulator model, this section will take the SiO_2 aerosol particles with radius of $r = 0.03$ mm (small particle radius) and $R = 0.06$ mm (large particle radius) as an example. The dielectric constant of the particles was kept constant, and the surface electric field strength of the composite insulator under six different spacings of 0–5r was calculated. The electric field distribution cloud diagram is shown in Fig. 12.

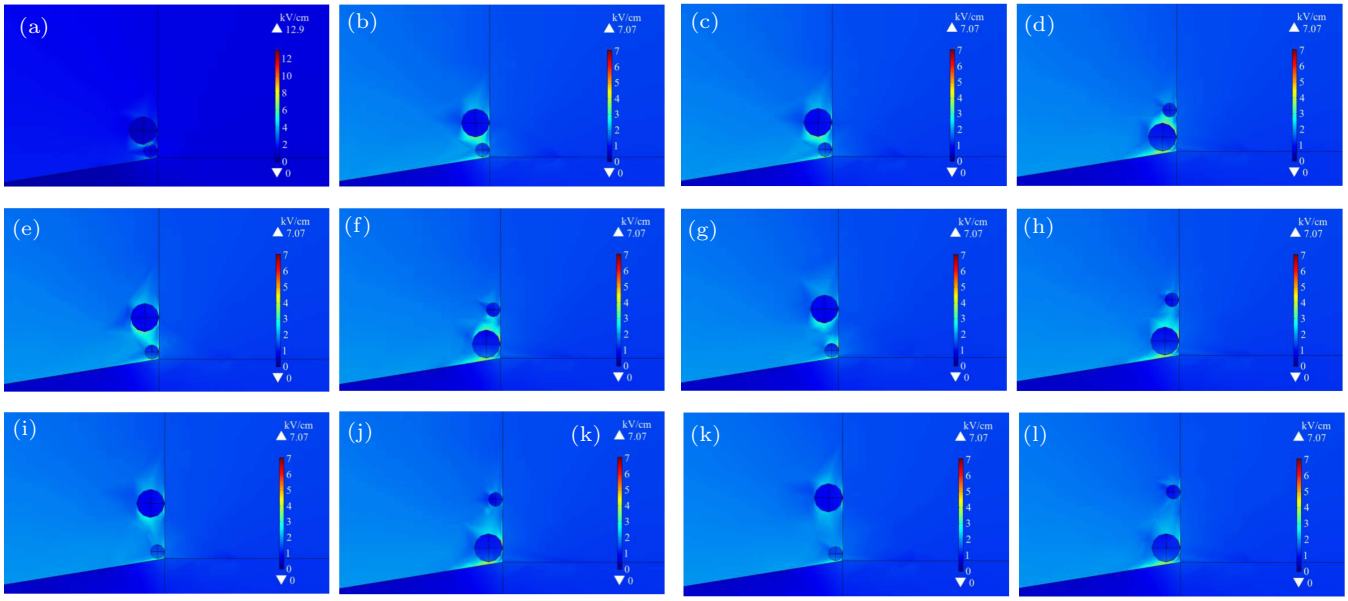


Fig. 12. The electric field distribution cloud diagram around unequal large particles under different spacings: (a) small–large arrangement ($d = 0$), (b) large–small arrangement ($d = 0$), (c) small–large arrangement ($d = r$), (d) large–small arrangement ($d = r$), (e) small–large arrangement ($d = 2r$), (f) large–small arrangement ($d = 2r$), (g) small–large arrangement ($d = 3r$), (h) large–small arrangement ($d = 3r$), (i) small–large arrangement ($d = 4r$), (j) large–small arrangement ($d = 4r$), (k) small–large arrangement ($d = 5r$), (l) large–small arrangement ($d = 5r$).

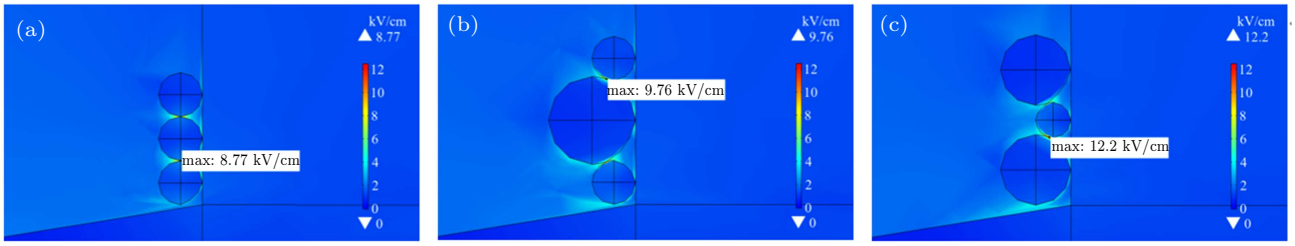
It can be seen from the field intensity distribution cloud diagram that when the distance between the two particles is equal, such as Figs. 12(e) and 12(f), the influence of large particles adsorbing small particles on the field strength around the insulator is greater than that of small particles adsorbing large particles, indicating that large particles have a stronger effect on the electric field on the surface of the insulator, and it is easier to adsorb small particles. Compared with the same situation, it can be obtained that the contact of particles (it is the case of zero spacing) has little effect on the electric field around the insulator, but the maximum electric field intensity on the surface of the particles is 1.3 times that of the electric

field when the two particles are in contact with the same size, which is about 4 times that of the electric field intensity under the action of single particles. With an increase in the distance between the double particles, the electric field strength between the particles shows a trend of increasing and then decreasing, indicating that when the distance between the particles reaches a certain distance, the interactions between the particles were almost 0. At this time, the influence of the double particles on the electric field on the surface of the insulator can be approximated as the operation of the single particles. For what has been studied in this section it can be concluded that SiO_2 particles of 2 times the size, with particle spacing greater than 5–6 times the radius of the small particles (approximately 3 times the radius of the large particle), have an effect that is almost zero, at which point the inter-particle electric field strength approximates the value of the original spatial field strength.

4.3. The influence of three-particle contamination layer on electric field distribution of insulator surface

4.3.1. The effect of chain arrangement of three particles

According to the calculation results of the double particle model, this section will take SiO_2 aerosol particles as an example to calculate the surface electric field strength of three particles with equal-sized, small–large–small size, and large–small–large sizes, respectively, which results in a cloud diagram of the surface field strength distributions as shown in Fig. 13.



(a) $r = 0.03$ mm (b) $r = 0.03$ mm, $R = 0.06$ mm (c) $R = 0.06$ mm, $r = 0.03$ mm

Fig. 13. The electric field distribution cloud diagrams around the three particles arranged in a chain, r is the radius of small particles and R is the radius of large particles in this section.

Comparing the results of the electric field distribution on the surface of the equal-sized double particles in contact with each other, it can be seen from Fig. 13(a) of the electric field distribution cloud map that the surface field strength of the particles will gradually decrease with the increase of the number of particles forming a chain. It can be inferred that if a chain of contamination layers is formed, the insulators surface electric field strength will be reduced, which will promote the prevention of pollution flashover on the surface of the insulator. With an increase in the number of large particles, the electric field strength between particles also gradually increases, indicating that large particles have a greater influence on the electric field strength between particles. Comparing Figs. 13(b) and 13(c), it can be found that the arrangement of small–large–small size has a greater influence on the electric field intensity of the insulator surface, and the average electric field intensity around it is about twice that of the arrangement of large size, indicating that the two sides of large particles are more likely to attract small particles. For Fig. 13(c), the arrangement of large–small–large size will produce a large field strength in the middle area of the particles, which is more likely to attract small particles or breakdown.

4.3.2. The influence of triangular arrangement of three particles

According to the calculation results of the double particle pollution model and the equal-sized chain arrangement model, this section will continue to take the SiO_2 aerosol particles with a radius of $r = 0.03$ mm as an example to study and analyze the influence of particles on the surface electric field of the insulator under the triangular stacking, and obtain the electric field distribution cloud picture as shown in Fig. 14.

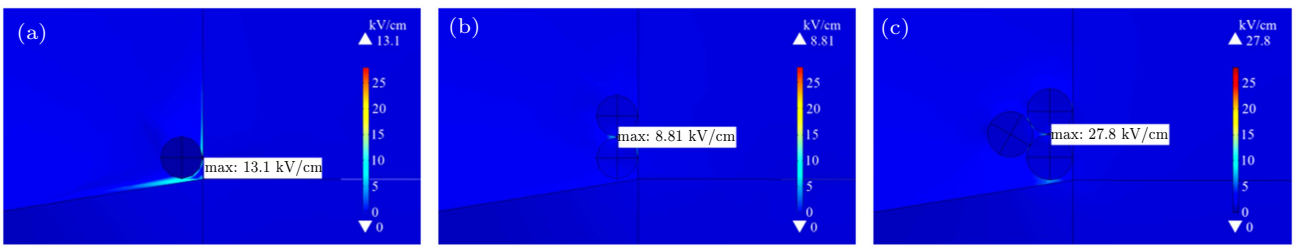


Fig. 14. The electric field distributions around the particle with different modes: (a) one particle, (b) two particles ($d = 0$), (c) three particles.

From the electric field distribution cloud diagram, it can be seen that the maximum electric field strength between the three particles arranged in a triangle is 27.8 kV/cm, the maximum electric field strength between the double particles is 8.81 kV/cm, and the maximum field strength around the single particle is 13.1 kV/cm, which leads to the conclusion that the maximum field strength of the triangularly arranged triple particles is approximately 2.12 times of that of the single particles, and about 3.16 times of that of the double particles that are in contact with each other, which indicates that the insulator surface adhering to the particles is more likely to be adsorbed in the field strength of the largest particles. Although the maximum field strength between the particles increases exponentially, the effect of the particles on the insulator surface is gradually reduced, from the double particles with a spacing of 0 to the triangular arrangement of the three particles, the electric field strength on the surface of the insulator is reduced by approximately 1/2, which suggests that the adsorption of multiple particles is conducive to the reduction of the insulator surface of the insulators, such as the occurrence of tarnish flash and breakdown and other phenomena affecting the safe operation of insulators.

4.4. The influence of wet environment on electric field distribution of insulator surface

The generation of electric field distortion on the surface of insulator is the root cause of flashover. In a humid environment, the air contains a large amount of water vapor, which changes the relative dielectric constant and conductivity of the air, thereby affecting the electric field intensity distribution on the surface of the insulator. However, when air pollution is serious, suspended particles in the atmosphere will affect the electric field distribution of the surrounding environment owing to their electrification and attachment to the surface of the insulator, which seriously jeopardizes the stable operation of the transmission system. Therefore, this section keeps the basic structural parameters of the model unchanged, and carries out a theoretical calculation of the electric field strength on the insulator surface for the particle condition when different pollution levels are adsorbed on the insulator surface in a humid environment, which provides a theoretical reference for the maintenance of the stability and safety of the transmission system.

Based on the research by Huang,[43] this section infers that when the relative humidity of the air reaches 100%, its relative dielectric constant is approximately 1.000747. At this point, the air is in a saturated humidity state, and contaminants are considered as fog droplets[44] with material parameter set to $\varepsilon_r = 81$, $\sigma = 0.6$ S/m. Additionally, according to the study by Jiang *et al.* on air pollution levels, air pollution was categorized into three levels: light pollution, heavy pollution, and catastrophic pollution. Under these conditions, the environmental conductivity is defined as the conductivity of fog water, which is set to 0.020 S/m, 0.219 S/m, 0.515 S/m.[45] The calculations were based on these parameters. In a humid environment with 100% relative humidity, the electric field strength on a clean insulator surface is calculated, and the resulting potential distribution and electric field distribution cloud diagrams are shown in Fig. 15.

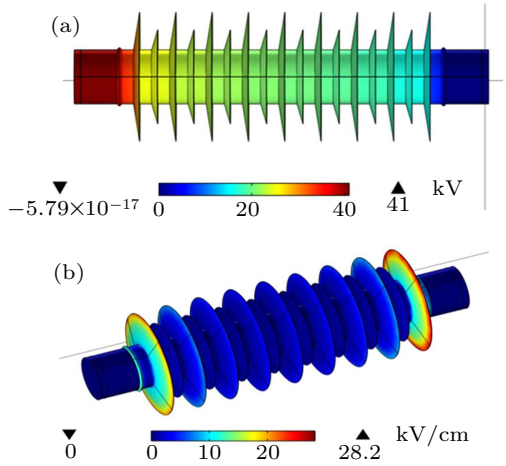


Fig. 15. The surface electric field and potential distribution of clean insulator in wet environment: (a) electric potential distribution, (b) electric field distribution.

Combined with Fig. 3, it can be seen that the overall potential of the insulator still shows the distribution characteristics of uniform radial distribution of potential and a decreasing axial distribution. The maximum electric field intensity on the surface of the insulator sheath under saturated moisture changes from 7.44 kV/cm to 28.2 kV/cm, which is three times larger than that under dry condition. It can be seen that the wet environment has a greater influence on the electric field on the surface of the insulator. Throughout the insulator, the electric field of the upper and lower umbrella skirts of the insulator in the damp saturated environment changes dramatically. The electric field intensity at the edge of the umbrella skirt was greater than that inside it, showing a decreasing trend along the transverse direction. The electric field intensity at the edge was about 2 times the electric field intensity at the inflection point.

In this section, the influence of three types of pollution layers on the electric field distribution of insulator surface in the above study under a wet environment is studied, and the change curve shown in Fig. 16 is obtained.

It can be observed from Fig. 16(a) that the value of the maximum electric field strength on the surface increases gradually with an increase in the particle radius, but the magnitude is relatively small. This indicates that, in a humid environment, the electric field distortion caused by charged particles is minimally affected by particle radius. The illustration of Fig. 16(b) shows that for the same particle radius, the

electric field strength on the surface of the saturated insulator decreases with increasing conductivity, but the difference is approximately ±10 kV/m. This suggests that under these air conditions, the electric field strength on the insulator surface is negatively correlated with the level of air pollution.

To more thoroughly reflect the relationship between contamination levels, particle spacing, and the electric field strength on the insulator surface, this section calculates and plots the electric field strength variation curves as shown in Figs. 16(c) and 16(d). Given that the variation patterns of the electric field for the three pollution levels are consistent, this section selects the scenario with the lowest pollution level ($\sigma = 0.020$ S/m) for detailed analysis. The inset in Fig. 16(c) indicates that at equal spacing, the electric field strength on the insulator surface gradually decreases with increasing pollution levels. Figure 16(d) shows that for the same pollution level, the electric field strength on the insulator surface is significantly influenced by the particle spacing. The field strength decreases gradually as the particle spacing increases, eventually stabilizing. However, the range of the surrounding field strength changes more drastically. This phenomenon may be due to the decreasing influence of mutual interactions between the particles as their spacing increases. Beyond a certain distance, the particles can be considered as "isolated particles", which subsequently affect the surface field strength of the insulator.

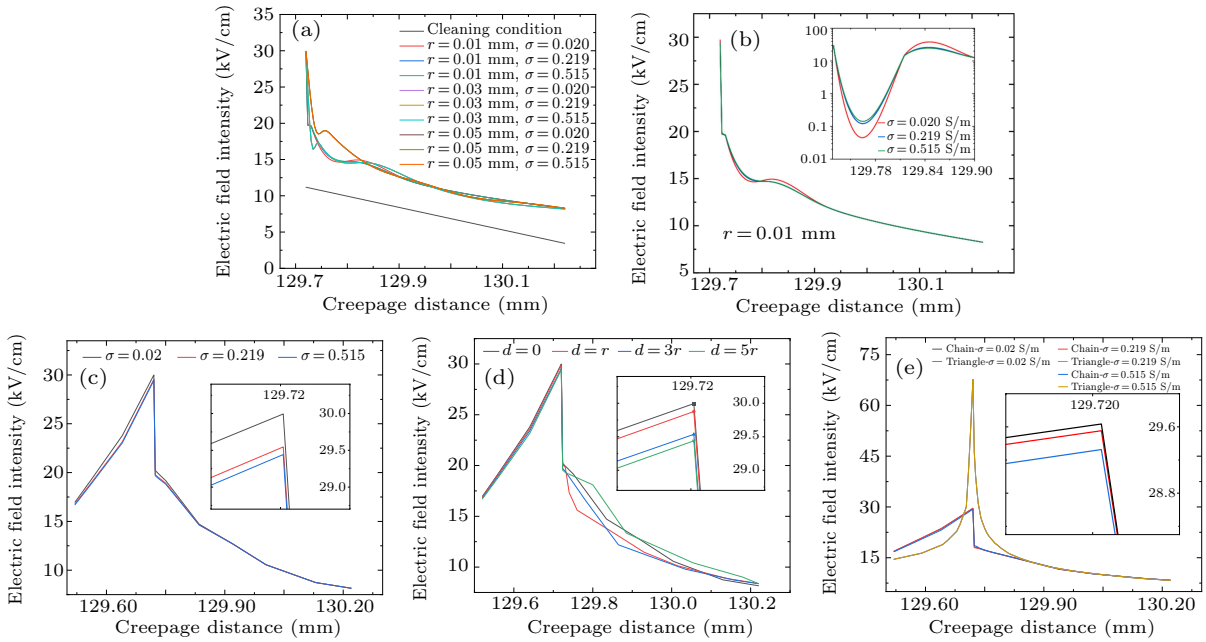


Fig. 16. The variation of electric field intensity on insulator surface under the influence of different pollution layers in humid environment: (a) field strength at the top of a single particle with the creepage distance, (b) variation of electric field with σ when $r = 0.01$ mm, (c) $r = 0.01$ mm, $d = 0$, (d) $r = 0.01$ mm, $\sigma = 0.020$ S/m, (e) variation of the field strength at the top of the three particles with the creepage distance.

The two particles in mutual contact in a humid environment can significantly affect the electric field on the insulator surface. Based on this, this section investigates the electric field strength on the insulator surface with a three-particle structure. The resulting variation curves of the electric field strength along the creepage distance are shown in Fig. 16(e). It is evident that a triangular arrangement of the contamination layer causes substantial electric field distortion on the insulator surface, with the maximum field strength reaching approximately 70 kV/cm, about 2.3 times the maximum field strength observed in a chain arrangement. This indicates that the triangular contamination layer is highly prone to tip discharge, which leads to air breakdown. Since the top particle in the triangular contamination layer is not on the insulator surface, the effect of different pollution levels on the insulator surface are nearly identical in the triangular arrangement. The inset in Fig. 16(e) shows that the surface electric field strength in the chain arrangement decreases with increasing conductivity. In summary, a triangular arrangement is more likely to cause wet flashover of the insulator, whereas the contamination layer of the chain arrangement has a broader impact range on the insulator surface and is more prone to adsorbing fine particles.

5. Conclusion

This study utilizes numerical simulations to explore how the electric field strength varies on insulator surfaces impacted by single-particle contamination of different sizes and materials, double-particle contamination with different spacings and sizes, and triple-particle contamination organized in different patterns and sizes. Additionally, this paper examines how the electric field on insulator surfaces changes in humid environments after contamination deposition. The major findings are summarized as follows.

(i) In the case of single-particle contamination, the elec-

tric field strength at the tip of the particle increases with increasing particle size until it stabilizes. For contaminants with varying compositions, the electric field strength at the apex of the particle increased linearly with the relative dielectric constant.

(ii) For double-particle contamination with equal particle sizes, the electric field strength on the insulator surface diminishes as the distance between the particles increases. For particles of different sizes, the simulation results suggest that larger particles are more likely to attract smaller charged particles within the radius of the larger particles.

(iii) The research demonstrates that the electric field generated by particles arranged in a triangular configuration is nearly twice as strong as that produced by particles in a linear arrangement. Both the configurations decreased the surface electric field strength. The triangular setup reduces the initial electric field strength by approximately 50%, indicating that both chain and triangular formations are effective in mitigating the flashover and breakdown risks.

(iv) In the three-dimensional composite insulator model under moisture-saturated, the maximum electric field strength on the insulator surface increases from 7.44 kV/cm under dry conditions to 28.2 kV/cm, representing a nearly threefold rise. This illustrates that humid conditions have a considerable effect on the surface electric field strength. Moreover, as the conductivity increased (suggesting greater pollution levels), the surface electric field strength progressively declined.

These results have significant practical implications for predicting the risk of contamination flashover in insulators and ensuring the safe operation of transmission lines.

Acknowledgements

Project supported by the National Natural Science Foundation of China (Grant Nos. 12064034 and 11562017), the Leading Talents Program of Science and Technology Innovation in Ningxia Hui Autonomous Region, China (Grant No. 2020GKLRLX08), and the Natural Science Foundation of Ningxia Hui Autonomous Region, China (Grant No. 2024AAC05040).

References

[1] Liu Z, Bi W, Chen X, Chen J, Qi D and Jiao Y 2020 *Insulators and Surge Arresters* **4** 228
[2] Kohei Y and Hiroya H 2018 *IEEE Electrical Insulation Magazine* **35** 23
[3] Takuma T, Ikeda T and Kawamoto T 1981 *IEEE Transactions on Power Apparatus and Systems* **100** 4802
[4] Li Y, Yang H, Zhang Q, Yang X, Yu X and Zhou J 2014 *IEEE Transactions on Dielectrics and Electrical Insulation* **21** 1735
[5] 1992 *Hybrid Transmission Corridor study*, Report
[6] Hoppel 1980 *Study of drifting, charged aerosols from HVDC lines*, Report
[7] He B, Zhao H, Chen C, Liu S and Peng Z 2017 *IEEE Transactions on Dielectrics and Electrical Insulation* **24** 2432
[8] Cui J, Su Z, Che W, Fan J, Liu X, Wu G and Zhao F 2001 *Electrical Equipment* **4** 6
[9] Wang J 2022 *Study on Multi-physical Field Analysis and Pollution Flashover Prediction of Catenary Insulator in Saline-alkali Area*, M.D. Thesis (Lanzhou Jiaotong University)
[10] Wang J, Liang X D and Liu Y *Proceedings of 2011 International Conference on Energy and Environment*, January 27, 2011, Shenzhen, China, p. 271
[11] Zhao Y, Hu Y, Jiang X, liu H and Shen H 2024 *Journal of Electronic Measurement and Instrumentation* **37** 186
[12] Wang J, Liang X D, Chen L H and Liu Y 2011 *Annual Report Conference on Electrical Insulation and Dielectric Phenomena*, October 16–19, 2011, Cancun, Mexico, p. 373
[13] Sun H 2017 *Study on Dynamic Contamination Depositing Characteristics of Insulators Using Coupled DEM and CFD Methods*, M.D. Thesis (Southwest Jiaotong University)
[14] Jiang M, Guo J, Jiang Y, Li L and Lu M 2020 *Environmental Science and Pollution Research* **27** 23643
[15] Ma Z, Li Y, Wu Y and Li G 2020 *Insulating Materials* **53** 90
[16] Lu T, Sun N, Su Z and Ma W 2021 *Southern Power System Technology* **15** 46
[17] Liu Y, Wu G, Guo Y, Zhang X, Liu K, Kang Y and Shi C 2020 *International Journal of Electrical Power & Energy Systems.* **115** 105447
[18] Lu J, He K, Ma X, Ju Y and Xie L 2015 *Proceedings of the CSEE* **35** 6222
[19] Kumar K B and Thomas M J 2016 *IEEE Transactions on Dielectrics and Electrical Insulation* **23** 974
[20] Peng S, Wu G and Shao M 2017 *High Voltage Apparatus* **53** 110
[21] Gao T, Hu Y, An Y, Xian R and Hou F 2019 *Insulating Materials* **52** 59
[22] Hu Q, Xia H, Jiang X, Liu M, Li Y and Zhu M 2020 *Proceedings of the CSEE* **40** 6027
[23] Xiang Y, Guo J and Luo Z 2011 *Southern Power System Technology* **5** 72
[24] Yu K 2019 *China Electrical Equipment Industry* **5** 76
[25] Lv Y, Wang J, Song Q and Liu Y 2021 *Power System Technology* **45** 1201
[26] Gao B, Zhang Y, Wang Q, Zhou J and Zhang Q 2008 *Insulators and Surge Arresters* **3** 13
[27] Xu Z, Lv F, Li H and Liu Y 2011 *High Voltage Engineering* **37** 944
[28] Liu Y, Zong H, Gao S and Du B 2020 *International Journal of Electrical Power & Energy Systems* **121** 106176
[29] Qiao X, Zhang Z, Jiang X, Sundararajan R, Ma X and Li X 2020 *International Journal of Electrical Power & Energy Systems* **120** 105993
[30] Fujii O, Honsali K, Mizuno Y and Naito K 2009 *IEEE Transactions on Dielectrics and Electrical Insulation* **16** 116
[31] Abd Rahman M, Izadi M and Ab Kadir M 2014 *IEEE International Conference on Power and Energy (PECon)*, pp. 113–118
[32] Ndoumbe J, Beroual A and Imano A M 2015 *IEEE Transactions on Dielectrics and Electrical Insulation* **22** 2669
[33] Krzma A S and Khamaira M Y 2018 *Elixir Elec. Engg.* **116** 50009
[34] Aouabed F, Bayadi A, Rahmani A E and Boudissa R 2018 *IEEE Transactions on Dielectrics and Electrical Insulation* **25** 413
[35] Salem A A and Abd-Rahman R *J. Phys.: Conf. Ser.* **1049** 012019
[36] reza Ahmadi-veshki M, Mirzaie M and Sobhani R 2020 *International Journal of Electrical Power & Energy Systems* **117** 105679
[37] Kim T, Sanyal S, Rabelo M and Yi J 2022 *ECS Journal of Solid State Science and Technology* **11** 073007
[38] Fadaeeasrami H, Faghihi F, Olamaei J and Mohammadnezhadshourkaei H 2022 *International Journal of Electrical Power & Energy Systems* **142** 108274
[39] Liu Y, Li X, Wang J, Ma X and Sun W 2024 *Chin. Phys. B* **33** 014101
[40] Li C and Lv B 2024 *High Voltage Apparatus* **60** 147
[41] Wang S, Wang J, Zhao L and Chen L 2021 *Electric Power* **54** 149
[42] Wan Q 1982 *Mining Safety & Environmental Protection* **1** 17
[43] Huang Z 1996 *Journal of Communication University of China (Science and Technology)* **7** 3
[44] Zhang C, Hu J and Li J 2018 *IET Generation, Transmission & Distribution* **12** 406
[45] Jiang X and Li Y 2014 *Power System Technology* **38** 576